

Article

Microstructural and Mechanical Properties of a Heat-Treated EV31A Magnesium Alloy Fabricated Using the Stir-Casting Process

M. Somasundaram  and U. NarendraKumar * 

Department of Manufacturing Engineering, School of Mechanical Engineering, Vellore Institute of Technology, Vellore 632 014, Tamil Nadu, India

* Correspondence: u.narendrakumar@vit.ac.in

Abstract: This study aims to prepare a stir-cast EV31A magnesium alloy and investigate the effects of the T4 condition (solid solution strengthening) and T6 condition (solid solution strengthening cum age hardening) on the phases, microstructure, mechanical properties, and fractography. The solid solution at 520 °C for 8 h allows the Rare-Earth Elements (REE) to dissolve in the Mg matrix, but the solubility is limited by the presence of Zn. This phenomenon is responsible for the T4 heat-treated alloy's strengthening, which raises the UTS to 212 MPa. The formation of new grains within the grains causes an increase in grain boundaries and dislocations during the T6 heat treatment process, increasing the strength (UTS) of the EV31A alloy to 230 MPa. In all three test conditions, the fractography of tensile samples revealed a cleavage-ductile/mixed mode fracture. As expected, the fine-grained T6 sample exhibited superior strengthening at the expense of ductility.

Keywords: stir casting; magnesium alloy; EV31A; mechanical properties; heat treatment



Citation: Somasundaram, M.; NarendraKumar, U. Microstructural and Mechanical Properties of a Heat-Treated EV31A Magnesium Alloy Fabricated Using the Stir-Casting Process. *Crystals* **2022**, *12*, 1163. <https://doi.org/10.3390/cryst12081163>

Academic Editors: Erdem Karakulak, Huseyin Sevik and Shouxun Ji

Received: 20 July 2022

Accepted: 13 August 2022

Published: 18 August 2022

Publisher's Note: MDPI stays neutral with regard to jurisdictional claims in published maps and institutional affiliations.



Copyright: © 2022 by the authors. Licensee MDPI, Basel, Switzerland. This article is an open access article distributed under the terms and conditions of the Creative Commons Attribution (CC BY) license (<https://creativecommons.org/licenses/by/4.0/>).

1. Introduction

Magnesium (Mg) and its alloys have recently received increased attention as an alternative to conventional materials in aerospace and automotive applications due to their excellent strength-to-weight ratio, damping capacity, and electrical and thermal conductivity [1,2]. Despite the fact that Mg has a low density and has potential for a variety of applications, its use is limited due to its poor mechanical properties, high degradation rate, poor ductility, and formability in atmospheric conditions [3]. Adding alloying elements [4], thermo-mechanical treatments, and surface modifications [5,6] can improve Mg's mechanical and degradation properties [7–10]. Mg has a high affinity for oxygen, making it difficult to process at high temperatures [11,12]. Mg and its alloys can be processed more easily if they are processed in an inert gas atmosphere. Casting processes produce 90% of Mg-related products, but their application is limited. To broaden its application, mechanical properties at room and elevated temperatures must be evaluated [13]. Stir casting is another viable and adaptable method for preparing Mg alloy [14–16]. Rare-Earth Elements (REE) alloying in Mg improves the mechanical properties of the alloy system [17–19]. REE-Mg has been found to have superior mechanical and corrosion resistance compared to other Mg alloys, according to [20]. The service life of a Mg alloy can be extended through additional heat treatment by varying the temperature and holding time [21]. It has also been reported that alloying Nd and Gd increases Mg castability and precipitate strengthening. According to another study, adding Gd to the Mg-Nd-Zn system increases age-hardening responses [22]. Previously, the mechanical properties of sand-cast, sintered, and heat-treated EV31A alloys were investigated. In general, the mechanical behavior of the cast alloy is greatly influenced by the microstructure, casting defects, and heat-treatment conditions [23,24]. There have been very few studies reported on the properties of Elektron 21 or EV31A for a variety of

sand-casting applications in the past ten years, and as a result, the topic has not been thoroughly investigated. However, the primary focus of the research shift is on the processing and characterization of a yttrium (Y)-based magnesium alloy. However, a yttrium-based magnesium alloy, on the other hand, is difficult to work with in the foundry and can be quite expensive. As a result, the focus was renewed on developing a yttrium-free magnesium alloy [25,26]. A magnesium alloy containing Rare-Earth elements (REE), known as EV31A, is the goal of this research, which uses the stir-casting method to produce the alloy as well as to study the microstructural and mechanical properties of the alloy in both its as-cast and heat-treated T4 and T6 conditions.

2. Materials and Methods

2.1. Material Preparation

The alloy for the study was made using the stir-casting method. An induction furnace with an argon (Ar) atmosphere was used for the melting process. Alloy ingots of magnesium (Mg), neodymium (Nd), gadolinium (Gd), zinc (Zn), and zirconia (Zr) were heated to 650 °C in a furnace together. The details of the elemental composition are illustrated in Table 1. On a stirrer, the molten alloy was rotated at a speed of 600 revolutions per minute (RPM) for five minutes at a temperature of 800 °C. As previously demonstrated, pouring molten alloy at 720 °C produces the cast block of EV31A with dimensions of 245 mm × 215 mm × 30 mm [27]. First is solid solutionizing at 520 °C for 8 h, followed by hot water quenching at around 60 to 80 °C, then age-hardening at 200 °C for 16 h, followed by air cooling. Table 2 shows the heat-treatment conditions followed to prepare test specimens. Angelini et al. discovered that a solutionizing temperature of 520 °C is optimal for avoiding incipient melting and localized melting along grain boundaries. The Mg alloy system exhibits a positive strengthening effect at a temperature of 200 °C for up to 16 h before becoming stable for 48 h [28]. The stated solutionizing temperature, aging temperature, and time were used for this study.

Table 1. Elemental composition of EV31A Mg alloy.

Elements	Mg	Nd	Gd	Zn	Zr
Wt. (%)	95.3 ± 1.3	3 ± 0.5	1 ± 0.5	0.2–0.5	0.2–0.5

Table 2. Details of heat-treatment processes.

Heat Treatment Process	T4 Condition		T6 Condition	
	Temperature (°C)	Time (Hours)	Temperature (°C)	Time (Hours)
Solid Solutionizing	520	8	520	8
Water Quenching	60 to 80	1 min	60 to 80	1 min
Age-hardening	-	-	200	16

2.2. Phase and Microstructural Analysis

A 10 mm × 10 mm × 2 mm sample was ground using a series of SiC abrasive papers with grit sizes of 400, 600, 800, 1000, 1200, 1500, and 2000, followed by polishing in alumina-ethanol slurry. A picric-acidic solution (10 mL distilled water, 0.6 g picric acid, 5 mL acidic acid, and 10 mL ethanol) was used to etch the sample.

The phase constituent of the EV31A alloy was identified using an X-ray diffractometer (XRD) (Bruker, D8- Advance P-XRD) with CuK α (1.5406) radiation at a scanning interval of 20° to 90°. The linear intercept method was used to manually measure the size of the grains (ASTM E112-10). The microstructure of the different specimens was observed with an inverted optical microscope (Carl Zeiss and Axio Lab A1) and using a Field Emission-Scanning Electron Microscope (FE-SEM) (Thermo Fisher Scientific FEI Quanta 250 FEG)

equipped with Energy Dispersive Spectroscopy (EDS) (Oxford). The sample was prepared through ion milling and examined using a transmission electron microscope (TEM).

2.3. Mechanical Properties and Fractography

Wire-cut Electrical Discharge Machining was utilized in the preparation of the test specimens for evaluating the material's mechanical properties (EDM). A 20 mm × 10 mm × 5 mm sample size was cut and mounted in a hot mounting machine for microhardness analysis. The Vickers micro-hardness (HV) was measured using the micro-hardness testing machine (Matsuzawa mmt-x) with a 50 gf load and a 15 s dwell time. The tensile test was performed in a hydraulic universal testing machine (Instron 8801) with an ASTM E8 standard sample and a crosshead speed of 1 mm/s. The Charpy impact test was performed on an ASTM E23 sample (FIT 300D) in an impact-testing machine. The tensile and impact samples used to conduct tensile and Charpy impact tests are shown in Figure 1. Three test specimens were analyzed under the same test conditions to validate the results.



Figure 1. ASTM standard specimens for (a) Tensile test—ASTM E08; (b) Impact test—ASTM E23.

3. Results and Discussion

3.1. Density

Based on the Archimedes principle, the relative density of the EV31A Mg alloy is determined to be 97.4%. This decrease in relative density is primarily due to the formation of pores during the stir-casting process, which reduces the density by 2.6%. The porosity of the EV31A alloy can be attributed to REE agglomerations and gas entrapment [29]. In addition, the porosity gives rise to the initiation and propagation of cracks in the cast product [30]. The porosity of 4% is acceptable in cast products, as per standards [29,31].

3.2. Phase Analysis

XRD analysis reveals the presence of different phases in EV31A alloy. Six different phases, $Mg_{12}Nd$, $Mg_{41}Nd_5$, α -Mg, REE-Zn (Gd-Zn), Zn-Zr phase (Zn_2Zr_3), and Zn, are observed in Figure 2. The Zn_2Zr_3 phase is identified, and Zn is detected in the as-cast sample from which Zr is dissolved during T4 heat treatment. Mg and Zr have the same crystal structure (hexagonal close-packed (HCP)) and lattice parameters, which causes grain nucleation and high dissolution of Zr in Mg when compared to Zn [32,33]. Furthermore, because Zn is the grain-refiner in the EV31A alloy system, the solubility of the Zr phase is proportional to the percentage of Zn [34,35]. The $Mg_{41}Nd_5$ phase is wholly dissolved due to a solid solution. The $Mg_{12}Nd$ is difficult to dissolve in a solid solution because of its tetragonal structure [22]. The eutectic phases in EV31A are significantly dissolved during the T4 heat-treatment process. The Zn content in the Mg-REE alloy system increases the effectiveness of precipitate hardening by restricting the solubility of Nd in Mg [35,36]. The peak intensity of $Mg_{12}Nd$, α -Mg, and Gd-Zn phases in the T4 heat-treated sample is lesser than in the as-cast sample, which reveals the effectiveness of the heat-treatment process. The report says that the Nd has solid solubility of 1.87 wt.% in Mg at 520 °C; this is also the reason for the Mg-Nd eutectic phase in the T4 heat-treated sample [22]. The Zn_2Zr_3 , Zr phases, Gd-Zn, and $Mg_{12}Nd$ peaks seen in the T6 heat-treated sample are very similar to the phases seen in the T4 heat-treated sample. Furthermore, at 548 °C, Gd solubility in Mg alloy is 23.49 wt.%, which falls exponentially as the temperature rises. Furthermore, Gd is 23.49 wt.% soluble in Mg alloy. At 548 °C, it decreases exponentially with temperature. Its solubility at 200 °C is 3.82 wt.%. Therefore, a Gd-based Mg alloy is an ideal system for age-hardening [37,38]. The prolonged heating at 200 °C leads to decomposition and replacement of the γ phase [22].

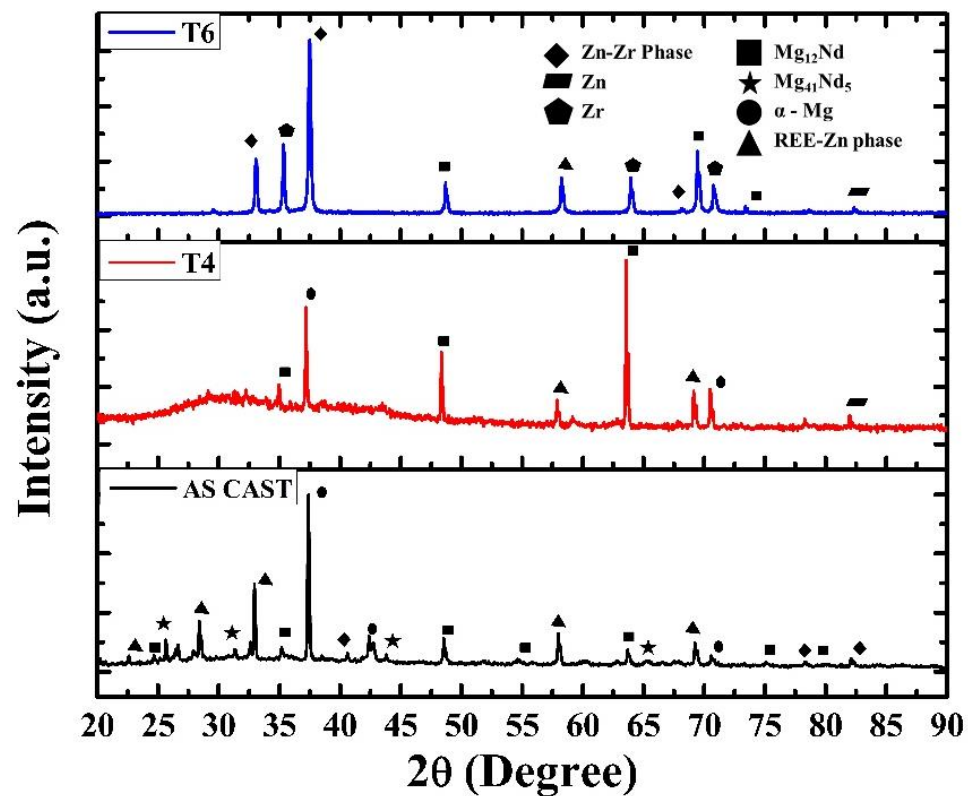


Figure 2. XRD patterns of EV31A in as-cast (black); T4 (red); T6 (blue) conditions.

3.3. Microstructure Analysis

The grain size of the samples is measured manually by the linear-intercept method using optical microscopy images, as shown in Figure 3a–c. The average grain size of as-cast, T4, and T6 heat-treated samples are $43.67 \pm 3.31 \mu\text{m}$, $67.51 \pm 1.82 \mu\text{m}$, and $37.16 \pm 2.02 \mu\text{m}$, respectively. The heat treatment of as-cast EV31A Mg alloy increases the grain size; further aging of the sample controls grain growth and decreases grain size. During the quenching process, the formation of new intermetallic phases inside the grain is noted in Figure 3b, which leads to the formation of new grain boundaries during the aging process, resulting in grain size reduction. Figure 3d–f shows an FE-SEM image in the Back-Scattered Electron mode (BSE) that reveals the microstructure of the as-cast and heat-treated samples. Figure 3d depicts the presence of α -Mg trapped in the as-cast samples' eutectic phase. Because grain boundaries are more chemically reactive than grains, alloying elements (impurities) are agglomerated along them. Regardless of phase-in, grain growth is observed in the T4 sample. The continuous growth of strain-free grains at elevated temperatures ($520 \text{ }^\circ\text{C}$ for 8 h) resulted in grain growth at the expense of smaller grains. The eutectic phase in the as-cast sample was dissolved after 8 h of heating at $520 \text{ }^\circ\text{C}$, and needle-shaped discontinuous eutectic phases were observed, as shown in Figure 3e. Heating samples caused precipitation within the coarser grains to form after the solution's heat treatment to an intermediate temperature of $200 \text{ }^\circ\text{C}$ for 16 h. As shown in Figure 3f, the age-hardening process significantly reduced the grain size through precipitation and segregation of the eutectic phase along the grain boundary.

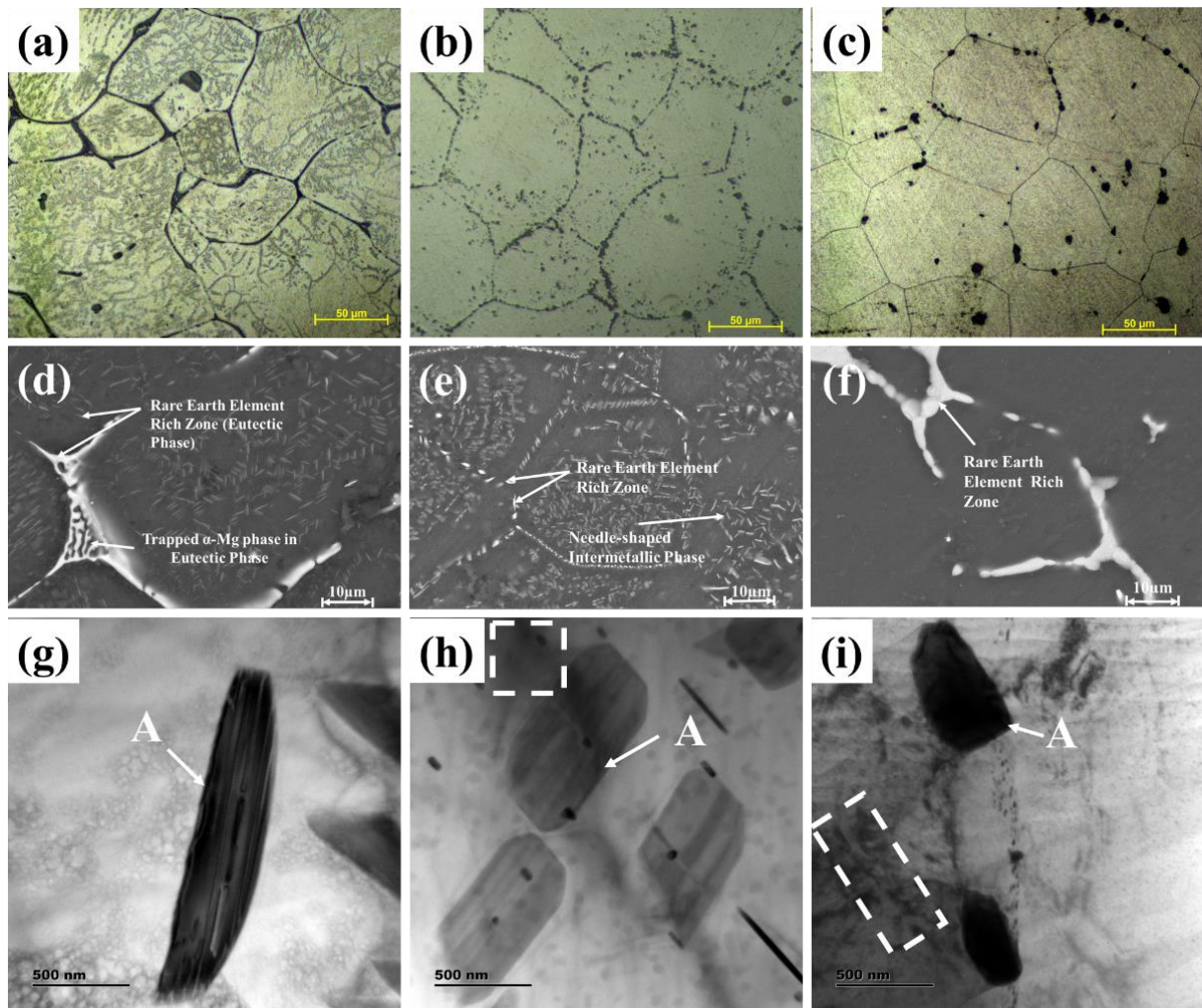


Figure 3. (a–c) Optical micrographs; (d–f) FE-SEM micrographs of EV31A; (g–i) Precipitates in studied alloy—TEM analysis. (a,d,g) As-cast; (b,e,h) after T4 heat-treatment; (c,f,i) after T6 heat-treatment. “A” point in Figure 3 (g–i) represents the precipitates, and the white rectangle in Figure 3 (h) and (i) represents dislocations.

Our previous study [27] shows the selected area diffraction (SAED) pattern under three test circumstances. First, the SAED pattern of the as-cast sample with miller indices of 304 and 602 indicates the GdZn and Mg₁₂Nd phases, respectively. The presence of Mg-Zn and GdZn phases in the T4 heat-treated sample and the existence of GdZn, Zr, and Mg-Zn phases in the T6 sample are also confirmed. Finally, Figure 3g–i depicts the test samples’ precipitates and dislocations. From the TEM analysis, it is understood that the dislocations are incorporated only after the heat-treatment processes, and dislocation density is high in the case of the T6 heat-treated alloy. As shown in Figure 4a–f, the EDS mapping of the aged sample confirms the existence of REE along the grain boundaries. In addition, the EDS study’s spot analysis reveals quantitative details about the composition of the alloy materials in that specific location, as shown in Figure 4g,h. It also confirms that Nd’s existence is higher along the grain boundaries than with Gd.

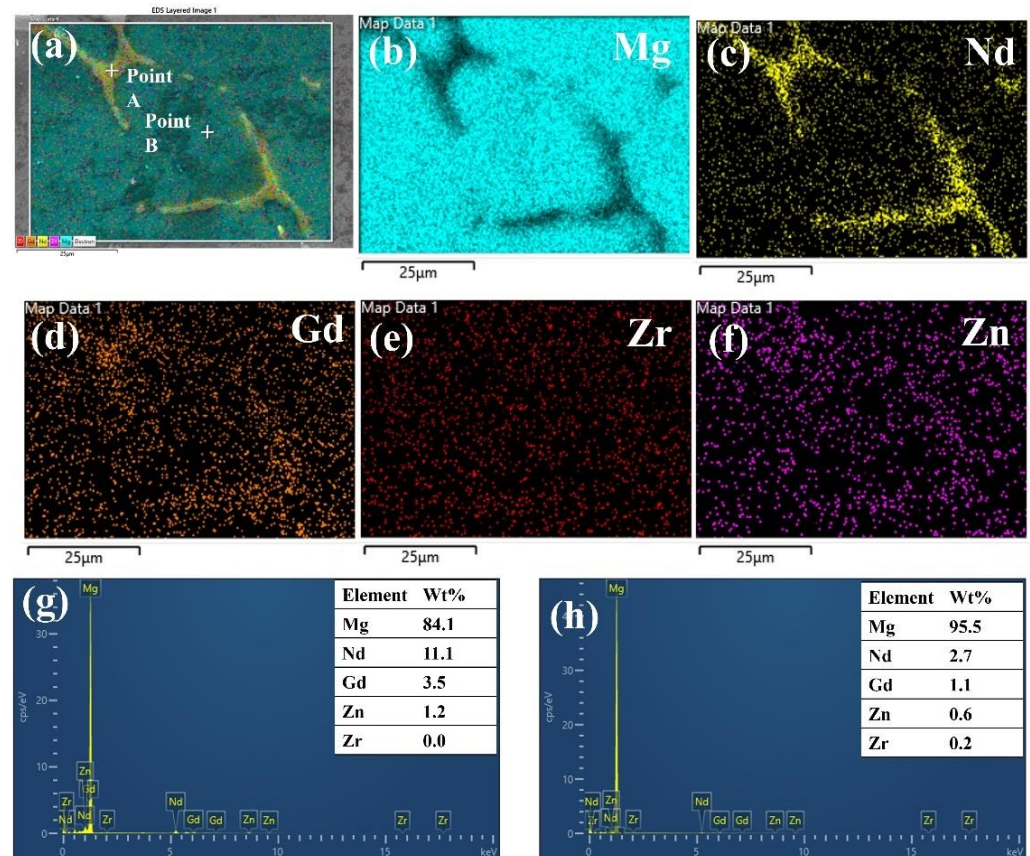


Figure 4. (a) SE micrograph of T6 heat-treated sample and EDS mapping of (b) Mg, (c) Nd, (d) Gd, (e) Zr, (f) Zn. EDS point analysis of (g) Point A and (h) Point B.

3.4. Mechanical Properties Analysis

The microhardness of the stir-cast sample was significantly higher than that of the sand-cast and sintered EV31A alloy [23,24]. The microhardness of the as-cast EV31A Mg alloy is 83 ± 8.38 HV_{0.05}, and it is 9.64% lesser than the T4 sample. The increase in microhardness is due to homogeneity improvement and secondary phase redistribution [24]. The age-hardened sample shows an 18.07% and 7.69% increase in microhardness compared with the as-cast and T4 heat-treated alloy. Tensile properties of the EV31A alloy are estimated using UTM with a crosshead speed of 1 mm/min. For the as-cast T4 and T6 samples, yield strength (YS) and ultimate tensile strength (UTS) increase while ductility decreases, respectively. The as-cast sample shows a yield strength (YS) of 130 ± 5.4 MPa compared with the YS of T4 and T6 heat-treated samples, which are increased by 10% and 33.08%. The UTS of the T6 heat-treated sample is 230 ± 8.7 MPa, which is 19.8% and 8.49% higher than the as-cast and T4 heat-treated samples. As-cast and T4 heat-treated alloy ductility is 28.57% and 16.67% higher than the T6 heat-treated sample, $5 \pm 0.52\%$.

By measuring the energy absorbed by the alloy, the Charpy impact test is used to determine the impact toughness of the EV31A alloy. Compared to the as-cast alloy, which has an impact strength of 3.7 ± 0.21 J, the T4 and T6 heat-treated alloys show an 18.92% and 43.24% increase in impact strength, respectively. Table 3 shows the mechanical properties of the EV31A alloy. The as-cast EV31A Mg alloy, trapped α -Mg, and Eutectic phases such as Mg₁₂Nd and Mg₄₁Nd₅ are segregated along grain boundaries; increasing the stress concentration in that vicinity is responsible for uneven deformation and premature failure [23,39]. Only secondary phase and grain boundary strengthening mechanisms contribute to stir-cast EV31A alloy [40]. Because Nd is less soluble in the alloy system, solution heat treatment has a more substantial effect [35,36]. The presence of Zn in the alloy system reduces solubility, which also corresponds to the Hume-Rothery conditions. The

more significant the difference in radius between Mg and REE solute atoms, as well as the higher concentration of REE solute, the better the mechanical properties of the EV31A alloy [41]. The grain boundary and solid solution strengthening mechanisms correspond to the T4-heated EV31A alloy strengthening [40]. During the aging process, the supersaturated solid solution's controlled decomposition to precipitation occurs in the Mg alloy system, resulting in a relatively larger nominal grain size. The smaller the grain size, the greater the surface area to volume ratio, and the greater the number of grain boundaries and dislocations per unit volume [22,42]. According to the Mg-Nd phase diagram [37,43], the solubility of Nd at the temperature of 200 °C is nearly equal to zero, so the effect of solid solution strengthening is ignored in the case of age hardening. Thus, only grain-boundary and precipitate-strengthening mechanisms are responsible for the strengthening behavior of the age-hardened EV31A alloy.

Table 3. Mechanical properties of EV31A Mg alloy.

Sample ID	Grain Size (μm)	Hardness ($\text{HV}_{0.05}$)	YS (MPa)	UTS (MPa)	Ductility (%)	Impact (J)
As-cast	44 ± 3.3	83 ± 8.4	130 ± 5.4	192 ± 10.3	7 ± 0.7	3.7 ± 0.2
T4	68 ± 1.8	91 ± 5.5	143 ± 6.7	212 ± 9.1	6 ± 0.5	4.4 ± 0.5
T6	37 ± 2.0	98 ± 4.1	173 ± 1.4	230 ± 8.7	5 ± 0.5	5.3 ± 0.5

3.5. Fractography

Figure 5a–c depicts and identifies the characteristics of brittle fractures—such as tear ridges, cleavage planes, and intergranular fractures—and ductile fractures, such as dimples. The cleavage fracture is associated with low-energy brittle fractures and produces bright, reflective facets. Even though the dimples are visible in all three conditions, the material's ductility decreases slightly as strength and hardness increase. Because of localized stress concentration, the eutectic compounds in the as-cast EV31A alloy are prone to failure. Furthermore, cracks in the eutectic phase spread through the soft grain interior by connecting micro-cracks, giving rise to intergranular cracks [40]. In the case of the T4 heat-treated sample, the crack initiation and propagation phenomenon is difficult to assess compared with the as-cast alloy because the dissolution of eutectic phases (Mg_{12}Nd , Mg_{41}Nd , GdZn) and the formation of non-continuous needle-shaped eutectic phases give resistance to crack propagation. However, the phenomenon gives rise to the brittle mode of fracture and intergranular cracks, which is why the T4 heat-treated alloy has more brittle fracture features than the as-cast alloy. In addition, the T4 heat-treated sample has a larger cleavage plane, whereas the T6 sample has more tear ridges. Even though the identified fracture features in the T6 sample differ, the fracture pattern is the same as in the T4 heat-treated alloy. Pores are indicated by the dimples in the fracture surface, as illustrated in Figure 5. The coalescence of micropores and the subsequent plastic deformation of the intersections between the pores result in dimples [44]. The EV31A alloy fractured in a mixed or cleavage-ductile mode in all three test conditions. A previous study [16] reported the same fracture mode.

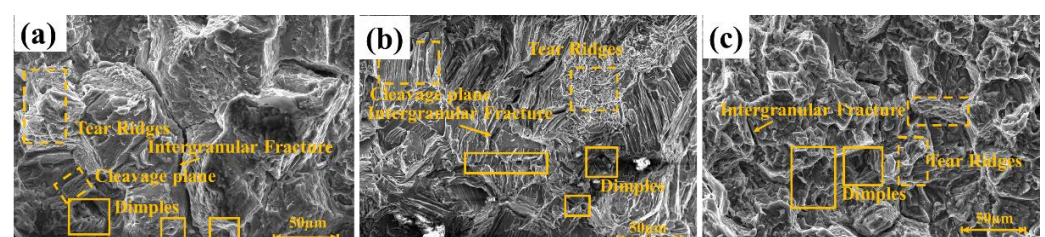


Figure 5. Fractography after tensile test of EV31A Mg alloy in SE mode of (a) As-cast; (b) T4, and (c) T6 conditions. (Solid rectangular box represents “Dimples”).

4. Conclusions

In this study, the EV31A Mg alloy is prepared using the stir-casting process, and the effect of stir casting and heat treatment (in both the T4 and T6 conditions) is investigated. The secondary phase and the grain boundary strengthening are both essential mechanisms that contribute to the strength of the alloy after it has been cast. Both the presence of non-continuous needle-shaped REE-rich zones on the grain boundaries of the T4 heat-treated alloy and the presence of supersaturated solutions are responsible for the enhancement of the material's mechanical properties. The T6 heat-treated samples shows the promising mechanical properties of $HV_{0.05} = 98 \pm 4.1$ HV; $YS = 173 \pm 1.4$ MPa; $UTS = 230 \pm 8.7$ MPa; $Ductility = 5 \pm 0.5\%$; $IS = 5.3 \pm 0.5$ J with a grain size of 37 ± 2.0 μm . The grain boundaries, Zn_2Zr_3 precipitates, and dislocations that are responsible for the strengthening of the T6 heat-treated EV31A alloy are increased as a result of the segregation of REE along the grain boundaries and the formation of new grains within the grains. Regardless of the conditions (as-cast; T4; T6), the fractography analysis revealed that the EV31A alloy displays a mixed-mode fracture. Eutectic phases influence the initiation, propagation, and failure of cracks in the EV31A alloy. The stir-casting method, followed by T6 heat treatment, is a potentially useful approach to producing EV31A alloy.

Author Contributions: Writing—original draft preparation, data curation, M.S.; formal analysis, U.N.; visualization, U.N.; writing—review and editing, M.S., U.N.; supervision, U.N. All authors have read and agreed to the published version of the manuscript.

Funding: This research received funding from School of Mechanical Engineering, Vellore Institute of Technology, Vellore.

Institutional Review Board Statement: Not applicable.

Informed Consent Statement: Not applicable.

Data Availability Statement: The raw/processed data required to reproduce these findings cannot be shared at this time as the data also form part of an ongoing study.

Acknowledgments: The authors would like to thank A. Raja Annamalai, Director, Centre for Innovation Manufacturing Research, Vellore Institute of Technology, Vellore, for introducing the area of research and aiding in fabricating the studied alloy. The authors would also like to acknowledge School of Mechanical Engineering, Vellore Institute of Technology, Vellore, for facilitating to conduct the study's experiments.

Conflicts of Interest: On behalf of all authors, the corresponding author states that there are no conflicts of interest.

References

1. Li, C.-J.; Sun, H.-F.; Li, X.-W.; Zhang, J.-L.; Fang, W.-B.; Tan, Z.-Y. Microstructure, texture and mechanical properties of Mg-3.0Zn-0.2Ca alloys fabricated by extrusion at various temperatures. *J. Alloys Compd.* **2015**, *652*, 122–131. [[CrossRef](#)]
2. Dvorský, D.; Kubásek, J.; Vojtěch, D.; Čavojský, M. Advanced Mechanical and Corrosion Properties of WE43 Alloy Prepared by Powder Metallurgy. *Acta Phys. Pol. A* **2018**, *134*, 748–752. [[CrossRef](#)]
3. Bettles, C.J.; Gibson, M.A. Material rate dependence and localized deformation in crystalline solids. *J. Miner. Met. Mater. Soc.* **2005**, *57*, 46–49. [[CrossRef](#)]
4. Bao, J.; Li, Q.; Chen, X.; Zhang, Q.; Chen, Z. Effect of Nd on the microstructure and corrosion behavior of Mg-Gd-Nd-Zr alloys. *Mater. Res. Express* **2021**, *8*, 046526. [[CrossRef](#)]
5. Zhang, X.; Cui, S.-D.; Zhou, L.; Lian, J.-B.; He, J.; Li, X.-W. Preparation and characterization of calcium phosphate containing coating on plasma electrolytic oxidized magnesium and its corrosion behavior in simulated body fluids. *J. Alloys Compd.* **2022**, *896*, 163042. [[CrossRef](#)]
6. Liu, L.; Dong, S.; Wang, F.; Chen, X.-B.; Dong, J. Fabrication of uniform and anti-corrosion layered double hydroxides film on Mg-Gd-Y-Zn-Zr alloy through solution pH tailoring. *Electrochim. Acta* **2022**, *411*, 140057. [[CrossRef](#)]
7. Gu, X.; Zheng, Y.; Cheng, Y.; Zhong, S.; Xi, T. In vitro corrosion and biocompatibility of binary magnesium alloys. *Biomaterials* **2009**, *30*, 484–498. [[CrossRef](#)]
8. Xu, L.; Zhang, E.; Yang, K. Phosphating treatment and corrosion properties of Mg-Mn-Zn alloy for biomedical application. *J. Mater. Sci. Mater. Electron.* **2009**, *20*, 859–867. [[CrossRef](#)]

9. Gu, X.; Xie, X.; Li, N.; Zheng, Y.; Qin, L. In vitro and in vivo studies on a Mg–Sr binary alloy system developed as a new kind of biodegradable metal. *Acta Biomater.* **2012**, *8*, 2360–2374. [[CrossRef](#)]
10. Feng, A.; Han, Y. The microstructure, mechanical and corrosion properties of calcium polyphosphate reinforced ZK60A magnesium alloy composites. *J. Alloys Compd.* **2010**, *504*, 585–593. [[CrossRef](#)]
11. Zhou, N.; Zhang, Z.; Dong, J.; Jin, L.; Ding, W. Selective oxidation behavior of an ignition-proof Mg–Y–Ca–Ce alloy. *J. Rare Earths* **2013**, *31*, 1003–1008. [[CrossRef](#)]
12. Aydin, D.; Bayindir, Z.; Hoseini, M.; Pekguleryuz, M. The high temperature oxidation and ignition behavior of Mg–Nd alloys part I: The oxidation of dilute alloys. *J. Alloys Compd.* **2013**, *569*, 35–44. [[CrossRef](#)]
13. Pan, F.; Yang, M.; Chen, X. A Review on Casting Magnesium Alloys: Modification of Commercial Alloys and Development of New Alloys. *J. Mater. Sci. Technol.* **2016**, *32*, 1211–1221. [[CrossRef](#)]
14. Moheimani, S.K.; Dackhah, M.; Mosallanejad, M.H.; Saboori, A. Fabrication and Characterization of the Modified EV31-Based Metal Matrix Nanocomposites. *Metals* **2021**, *11*, 125. [[CrossRef](#)]
15. Grilo, J.; Carneiro, V.H.; Teixeira, J.C.; Puga, H. Manufacturing methodology on casting-based alu-minium matrix composites: Systematic review. *Metals* **2021**, *11*, 436. [[CrossRef](#)]
16. Moussa, M.E.; El-Hadad, S.; Khalifa, W. Strengthening Effect of Y₂O₃ on AZ92 Magnesium Alloy Using Stir Casting Process. *Int. J. Met.* **2021**, *15*, 818–828. [[CrossRef](#)]
17. Xia, X.; Chen, Q.; Li, J.; Shu, D.; Hu, C.; Huang, S.; Zhao, Z. Characterization of hot deformation behavior of as-extruded Mg–Gd–Y–Zn–Zr alloy. *J. Alloys Compd.* **2014**, *610*, 203–211. [[CrossRef](#)]
18. Yu, H.; Park, S.H.; You, B.S.; Kim, Y.M.; Yu, H.S. Effects of extrusion speed on the microstructure and mechanical properties of ZK60 alloys with and without 1wt% cerium addition. *Mater. Sci. Eng. A* **2013**, *583*, 25–35. [[CrossRef](#)]
19. Park, S.H.; You, B.S.; Mishra, R.K.; Sachdev, A.K. Effects of extrusion parameters on the microstructure and mechanical properties of Mg–Zn–(Mn)–Ce/Gd alloys. *Mater. Sci. Eng. A* **2014**, *598*, 396–406. [[CrossRef](#)]
20. Prasad, S.S.; Prasad, S.B.; Verma, K.; Mishra, R.K.; Kumar, V.; Singh, S. The role and significance of Magnesium in modern day research—A review. *J. Magnes. Alloy.* **2021**, *10*, 1–61. [[CrossRef](#)]
21. Barylski, A.; Aniołek, K.; Dercz, G.; Kowalewski, P.; Kaptacz, S.; Rak, J.; Kupka, M. Investigation of Micromechanical Properties and Tribological Behavior of WE43 Magnesium Alloy after Deep Cryogenic Treatment Combined with Precipitation Hardening. *Materials* **2021**, *14*, 7343. [[CrossRef](#)] [[PubMed](#)]
22. Nie, J.-F. Precipitation and Hardening in Magnesium Alloys. *Metall. Mater. Trans. A* **2012**, *43*, 3891–3939. [[CrossRef](#)]
23. Qi, F.; Zhang, X.; Wu, G.; Liu, W.; He, X.; Ding, W. High cycle fatigue behavior and mechanical performance of a novel sand-cast Mg–Nd–Gd alloy: Effect of heat treatment. *Mater. Sci. Eng. A* **2021**, *813*, 141172. [[CrossRef](#)]
24. Jana, A.; Das, M.; Balla, V.K. Effect of heat treatment on microstructure, mechanical, corrosion and biocompatibility of Mg–Zn–Zr–Gd–Nd alloy. *J. Alloys Compd.* **2020**, *821*, 153462. [[CrossRef](#)]
25. Rokhlin, L.; Nikitina, N.; Dobatkina, T. Solid-state phase equilibria in the Mg corner of the Mg–Gd–Sm phase diagram. *J. Alloys Compd.* **1996**, *239*, 209–213. [[CrossRef](#)]
26. Kielbus, A.; Rzychoń, T.; Przeliorz, R. DSC and Microstructural Investigations of the Elektron 21 Magnesium Alloy. *Mater. Sci. Forum* **2010**, *638–642*, 1447–1452. [[CrossRef](#)]
27. Somasundaram, M.; Narendrakumar, U.; Annamalai, A.R. Effect of heat treatment on fatigue behaviour of stir-cast EV31A magnesium alloy. *Mater. Lett.* **2022**, *313*, 131721. [[CrossRef](#)]
28. Angelini, V.; Ceschini, L.; Morri, A.; Apelian, D. Influence of Heat Treatment on Microstructure and Mechanical Properties of Rare Earth-Rich Magnesium Alloy. *Int. J. Met.* **2017**, *11*, 382–395. [[CrossRef](#)]
29. Tian, C.; Li, X.; Li, H.; Guo, G.; Wang, L.; Rong, Y. The effect of porosity on the mechanical property of metal-bonded diamond grinding wheel fabricated by selective laser melting (SLM). *Mater. Sci. Eng. A* **2019**, *743*, 697–706. [[CrossRef](#)]
30. Sankhla, A.; Patel, K.M. Metal Matrix Composites Fabricated by Stir Casting Process—A Review. *Adv. Mater. Process. Technol.* **2021**, 1–22. [[CrossRef](#)]
31. Huang, S.-J.; Abbas, A. Effects of tungsten disulfide on microstructure and mechanical properties of AZ91 magnesium alloy manufactured by stir casting. *J. Alloys Compd.* **2020**, *817*, 153321. [[CrossRef](#)]
32. Emley, E. *Principles of Magnesium Technology*; Pergamon Press: New York, NY, USA; London, UK, 1966.
33. Qian, M.; Graham, D.; Zheng, L.; St John, D.H.; Frost, M.T. Alloying of pure magnesium with Mg 33.3 wt-%Zr master alloy. *Mater. Sci. Technol.* **2003**, *19*, 156–162. [[CrossRef](#)]
34. StJohn, D.H.; Qian, M.; Easton, M.; Cao, P.; Hildebrand, Z. Grain refinement of magnesium alloys. *Met. Mater. Trans. A* **2005**, *36*, 1669–1679. [[CrossRef](#)]
35. Freney, T.A.; Mishra, R.S. Effect of Friction Stir Processing on Microstructure and Mechanical Properties of a Cast-Magnesium–Rare Earth Alloy. *Met. Mater. Trans. A* **2010**, *41*, 73–84. [[CrossRef](#)]
36. Rokhlin, L.L. *Magnesium Alloys Containing Rare Earth Metals: Structure and Properties*; CRC Press: London, UK, 2003. [[CrossRef](#)]
37. Nayeb-Hashemi, A. *Phase Diagrams of Binary Magnesium Alloys*; ASM International: Metals Park, OH, USA, 1988; Volume 370.
38. Smola, B.; Stulíková, I.; von Buch, F.; Mordike, B. Structural aspects of high-performance Mg alloys design. *Mater. Sci. Eng. A* **2002**, *324*, 113–117. [[CrossRef](#)]
39. Li, Z.; Luo, A.; Wang, Q.; Peng, L.; Fu, P.; Wu, G. Effects of grain size and heat treatment on the tensile properties of Mg–3Nd–0.2Zn (wt%) magnesium alloys. *Mater. Sci. Eng. A* **2013**, *564*, 450–460. [[CrossRef](#)]

40. Peng, L.; Liming, P.; Haiyan, J.; Jianwei, C.; Chunquan, Z. Effects of heat treatments on the microstructures and mechanical properties of Mg–3Nd–0.2Zn–0.4Zr (wt.%) alloy. *Mater. Sci. Eng. A* **2008**, *486*, 183–192. [[CrossRef](#)]
41. Jiang, H.; Zheng, M.; Qiao, X.; Wu, K.; Peng, Q.; Yang, S.; Yuan, Y.; Luo, J. Microstructure and mechanical properties of WE43 magnesium alloy fabricated by direct-chill casting. *Mater. Sci. Eng. A* **2017**, *684*, 158–164. [[CrossRef](#)]
42. Davis, A.; Kennedy, J.; Lunt, D.; Guo, J.; Strong, D.; Robson, J. Preageing of magnesium alloys. *Mater. Sci. Eng. A* **2021**, *809*, 141002. [[CrossRef](#)]
43. Delfino, S.; Saccone, A.; Ferro, R. Phase relationships in the neodymium-magnesium alloy system. *Met. Mater. Trans. A* **1990**, *21*, 2109–2114. [[CrossRef](#)]
44. Konovalenko, I.; Maruschak, P.; Brezinová, J.; Brezina, J. Morphological Characteristics of Dimples of Ductile Fracture of VT23M Titanium Alloy and Identification of Dimples on Fractograms of Different Scale. *Materials* **2019**, *12*, 2051. [[CrossRef](#)] [[PubMed](#)]